

## TRACKING SIMULATION AND WIRE CHAMBER REQUIREMENTS FOR THE SSC\*

GAIL G. HANSON, BOGDAN B. NICZYPORUK<sup>†</sup> AND ANDREA P. T. PALOUNEK<sup>‡</sup>  
*Stanford Linear Accelerator Center, Stanford University, Stanford, California 94309*

### ABSTRACT

Limitations placed on wire chambers by radiation damage and rate requirements in the SSC environment are reviewed. Possible conceptual designs for wire chamber tracking systems which meet these requirements are discussed. Computer simulation studies of tracking in such systems are presented. Simulations of events from interesting physics at the SSC, including hits from minimum bias background events, are examined. Results of some preliminary pattern recognition studies are given.

### 1. INTRODUCTION

The primary motivation for the SSC is the expectation that it will lead to new discoveries, such as Higgs bosons, supersymmetric particles, heavy  $W$ 's or  $Z$ 's, new heavy fermions, or composite particles with masses in the TeV region. Such particles would be produced in the central rapidity region, that is, over  $\pm 3$  units of rapidity, and would decay to high- $p_T$  electrons, muons, or jets, often with large missing transverse energy ( $E_T$ ) due to undetectable neutrinos. In order to fully investigate the physics opportunities in this regime, a general-purpose detector which includes charged particle tracking is needed. Some of the most important functions of charged particle tracking include:

1. Identification of electrons.
2. Separation of multiple interactions within the same bunch crossing.
3. Matching electrons, muons, and jets to the correct vertex.
4. Electron charge sign determination.

\* Work supported by the Department of Energy, contract DE-AC03-76SF00515.

<sup>†</sup> Permanent Address: CEBAF, Newport News, Virginia 23606.

<sup>‡</sup> Present Address: Lawrence Berkeley Laboratory, Berkeley, California 94720.

5. Improving  $e/\pi$  separation.
6. Identification of secondary vertices.
7. Identification of  $\tau$  leptons.
8. Invariant mass or momentum cuts.
9. Improving the missing  $E_T$  measurement and verifying calorimeter data.
10. Establishing the credibility of new physics and providing redundancy.

Many of these functions require momentum measurement in a magnetic field.

Tracking at the SSC at the full design luminosity of  $10^{33} \text{ cm}^{-2}\text{s}^{-1}$  is expected to be a difficult problem. The limitations imposed by rates and radiation damage are severe. However, the dominant constraint is the combination of occupancy and double-hit resolution. Single events from new physics at the SSC have many (several hundred) charged particle tracks and are further complicated by curling tracks in a magnetic field, photon conversions, hits from events from out-of-time bunch crossings, and multiple interactions within the same bunch crossing. These problems can probably be solved, but at the cost of mechanical complexity and many signal channels.<sup>1)</sup> It has not been established how well one can find tracks in complex SSC events. We report here on a computer simulation study which addresses these problems.

### 2. WIRE CHAMBER REQUIREMENTS

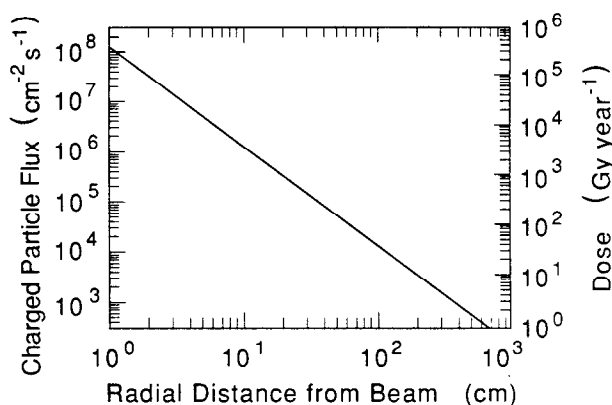
#### 2.1 The SSC Environment

The design luminosity,  $\mathcal{L}$ , of the SSC is  $10^{33} \text{ cm}^{-2}\text{s}^{-1}$  with an energy of 40 TeV in the center of mass. The inelastic cross section,  $\sigma$ , at 40 TeV is expected to be about 100 mb, which gives  $10^8$  interactions per second at the design luminosity. The bunch separation is 4.8 m, so the time between bunch crossings,  $t_B$ , is 16 ns, which leads to an

average number of interactions per bunch crossing,  $n_I$ , of 1.6 at the design luminosity. Most of these interactions are minimum bias events or low- $p_T$  hard scattering processes in which particle production is expected to be uniform in rapidity with an average charged particle multiplicity per unit of rapidity,  $n_c$ , of 7.5 over the rapidity range  $|\eta| < 6$ .<sup>2)</sup> Figure 1 (from Ref. 2) shows the resulting charged particle flux and annual dose as a function of perpendicular distance from the beam for standard SSC operating conditions.

## 2.2 Rates and Radiation Damage

Radiation damage and rate limitations impose severe constraints on charged particle tracking detectors at the SSC, as described in several references.<sup>1,3)</sup> These constraints are summarized here since they are necessary considerations for the design of any SSC tracking system.



10-88

6164A1

Fig. 1. The charged particle flux and annual dose as a function of perpendicular distance from the beam under standard SSC operating conditions (from Ref. 2).

A tracking system for the SSC is assumed to be made up of wires running (nearly) parallel to the beam line. The width,  $w$ , of the cell is assumed to be equal to the height,  $h$ , and the drift distance,  $d$ , is half the cell width. The ionization rate,  $\alpha$ , in the gas is assumed to be 100 electrons/cm. The gas gain,  $G$ , is assumed to be  $2 \times 10^4$ .

The flux of particles per unit length ( $\ell$ ) of wire in a cell at radius  $r$  is given by

$$\frac{d^2n}{d\ell dt} = \frac{n_c w \sigma \mathcal{L} \sin \theta}{2\pi r^2}, \quad (1)$$

where  $\theta$  is the angle relative to the beam direction. The ionization produced by a charged particle at angle  $\theta$  is  $h\alpha/\sin\theta$ , so the ionization per unit length of wire is independent of  $\theta$ . Thus the current draw per wire,  $I$ , for a

layer of wires of length  $L$  at radius  $r$  is given by

$$I = \frac{n_c w h \sigma \mathcal{L} G e \alpha L}{2\pi r^2}, \quad (2)$$

where  $e$  is the electron charge. A layer of 4 mm wide cells at a radius of 50 cm covering  $|\eta| < 1.5$  ( $L = 213$  cm) will draw  $0.52 \mu\text{A/wire}$ . The limit of acceptable current draw before breakdown will occur is about  $1 \mu\text{A/wire}$ .

Wire chamber lifetimes are measured in deposited charge per unit length of wire before a decrease in gain occurs. The decrease in gain is due to the buildup of material on the wires. For the above example of a 4 mm cell at 50 cm radius covering  $|\eta| < 1.5$ , the collected charge over a chamber lifetime of five years ( $5 \times 10^7$  s) would be  $0.12$  C/cm. Chamber lifetimes of  $1.0$  C/cm have been measured under very clean laboratory conditions.<sup>4)</sup> For the purposes of a realistic experiment, it is probably best to assume a chamber lifetime about an order of magnitude below this.

Changes in gain for wire chambers have been observed at the level of  $10^5$  particles/cm-s at a gas gain of  $\sim 4 \times 10^5$  due to space charge buildup.<sup>5)</sup> The particle flux is given by Eq. (1). For the above example of 4 mm wide cells at a radius of 50 cm, the flux would be  $1.9 \times 10^4$  particles/cm-s at  $\theta = 90^\circ$  where the flux is maximum. Since the gas gain must be much smaller than  $4 \times 10^5$  because of current draw and lifetime considerations, space charge should not be an important limitation.

The hit rate per wire,  $R$ , for SSC central tracking chambers is quite large and is given by

$$R = \frac{n_c \eta_{max} \sigma \mathcal{L} w}{\pi r} \quad (3)$$

for chambers covering  $|\eta| < \eta_{max}$ . Thus a 4 mm cell at 50 cm radius covering  $|\eta| < 1.5$  would have a hit rate per wire of 2.9 Mhz. Existing electronics can probably handle rates of  $\sim 10$  Mhz.

A very serious limitation for tracking systems at the SSC is occupancy. Since the time between bunch crossings at the SSC is shorter than the resolving time of a typical drift chamber cell, the cell is sensitive to several bunch crossings. The occupancy,  $O$ , is given by

$$O = \frac{2 n_c \eta_{max} n_I n_B d}{\pi r}, \quad (4)$$

where  $n_B$  is the number of bunch crossings during the resolving time of the cell.  $n_B$  is given by

$$n_B = 1 + \text{int} \left( \frac{t_R}{t_B} \right) \left[ 2 - \frac{t_B}{t_R} - \left( \frac{t_B}{t_R} \right) \text{int} \left( \frac{t_R}{t_B} \right) \right], \quad (5)$$

where  $t_R$  is the resolving time of the cell,  $d/v_D$ , for drift velocity  $v_D$ , and  $\text{int}(x)$  is the largest integer  $\leq x$ . Actually,  $n_B$  is very close to  $t_R/t_B = d/(v_D t_B)$ . A 4 mm

wide cell (2 mm drift) has a resolving time of 40 ns for a typical drift velocity of 50  $\mu\text{m}/\text{ns}$  and is therefore sensitive to 2.6 bunch crossings. A layer of such cells at a radius of 50 cm and covering a rapidity range  $|\eta| < 1.5$  would have an occupancy of 12% per cell. It is guessed that an occupancy of  $\sim 10\%$  is reasonable, but a realistic answer depends on the effects on pattern recognition and track finding, which are discussed in more detail in Section 3. Occupancy limits the cell width at any radius in a tracking system since, even at larger radius, as one increases the cell width the cell becomes sensitive to more bunch crossings. Since the occupancy increases quadratically with  $d$  and decreases linearly with  $r$ , the maximum cell size can increase only as the square root of the radius. A faster gas,<sup>6)</sup> such as mixtures of  $\text{CF}_4$  with a saturated drift velocity of 125  $\mu\text{m}/\text{ns}$ , would improve the situation considerably by giving lower occupancy for a given cell width.

One should keep in mind that these rates are based only on particles produced in an interaction and must be increased by a factor of 2–4 because of curling tracks in a magnetic field, converted photons, and albedo particles leaking out of the front face of the calorimeter. These limitations seriously affect the design of any SSC tracking device, regardless of pattern recognition considerations. For example, if one finds that an occupancy of 30% is reasonable for track finding, one cannot increase the cell width or move to a smaller radius without carefully considering the effects on current draw and chamber lifetime.

### 2.3 Tracking System Considerations

A large solenoid detector based on more-or-less "conventional" technology was discussed at the 1987 Berkeley Workshop.<sup>7)</sup> An examination of the requirements for momentum resolution based on the physics led to the criterion that the sign of the charge for electrons should be measured for  $p_T \leq 0.5\text{--}1.0$  TeV/c. The momentum resolution is given by<sup>8)</sup>

$$\frac{\sigma_{p_T}}{p_T^2} = \sqrt{\frac{720}{1 + 5/N}} \left( \frac{\sigma_x}{0.3 q B D^2 \sqrt{N}} \right), \quad (6)$$

where  $p_T$  is the transverse momentum of the particle in GeV/c,  $q$  is the charge in units of the electron charge,  $\sigma_x$  is the spatial resolution in m,  $B$  is the magnetic field in Tesla,  $D$  is the track length in m, and  $N$  is the number of measurements, assumed to be equally spaced. The outer radius for tracking was restricted to 1.6 m in order to place all of the calorimetry inside the magnet coil. The inner radius is constrained by the rate considerations discussed in the previous Section to 40–50 cm. A spatial resolution of 150  $\mu\text{m}$  was assumed. The magnet was a large superconducting solenoid with 2 Tesla field. With  $\sim 100$  measurements the momentum resolution which can be obtained

with such a system is  $0.54p_T$  (TeV/c) using only wires at radii larger than 50 cm. If the particles are constrained to come from the interaction region, the momentum resolution would improve to  $0.26p_T$ .

The tracking detector design for the Large Solenoid Detector was divided into central tracking ( $|\eta| \lesssim 1.2$ ) and intermediate tracking ( $1.2 \lesssim |\eta| < 2.5$ ). The central tracking chambers were assumed to have an inner radius of 40 cm, but only the layers at radii greater than 50 cm were expected to be operable at the full design luminosity. For the reasons discussed in the previous Section, the cell widths are constrained to a few mm. Straw tube chambers are a natural candidate for a small cell design. Construction possibilities for a central tracking system made of straw tubes are discussed in Refs. 1 and 9. A central tracking system based on jet cells, such as shown in Fig. 2, might also be considered. However, since the jet cell would be only a few mm wide and would be tilted so that the electron drift trajectories in the 2 Tesla magnetic field would be perpendicular to the sense wire planes, the advantages of a jet cell, e.g., uniform drift electric field over most of the cell and long track segments in one cell, are lost. In addition, there would be large forces on the endplates due to the tension of the large number of field wires. Also, as in any open wire geometry, it would be difficult to devise a mechanism to support the long sense wires in order to maintain electrostatic stability.

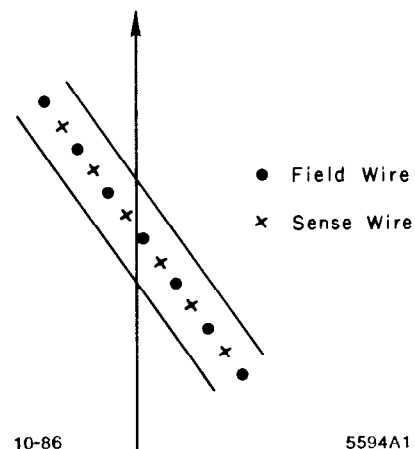


Fig. 2. Narrow tilted jet cell with radial track.

The central tracking system for the Large Solenoid Detector was assumed to be built of straw tubes of radii from 2 to 3.5 mm parallel or nearly parallel to the beam direction. The straws are made of aluminized polyester film (Mylar) or polycarbonate (Lexan) with wall thicknesses of about 30  $\mu\text{m}$ . The straws were assumed to be at atmospheric pressure. Eight layers of straws are glued together to form superlayers. Within each superlayer the layers are staggered by half the cell width in order to allow hits from

out-of-time bunch crossings to be rejected and resolve left-right ambiguities, as illustrated in Fig. 3. By dividing the chamber into eight-straw-thick superlayers locally identifiable track segments can be obtained with a high level of redundancy. Every other superlayer is small-angle stereo ( $\sim 3^\circ$ ) in order to measure the coordinate along the wire.

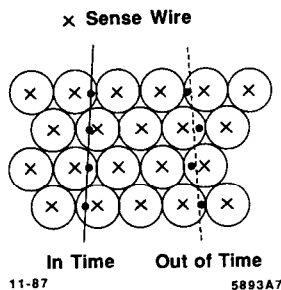


Fig. 3. Layers of straw tubes in a superlayer with every other layer staggered by the straw tube radius. A single in-time track will appear as a series of hits on the wires on alternate sides of the track. The left-right ambiguity is easily resolved locally. A track from an out-of-time bunch crossing will produce hits which are displaced from possible tracks by at least 16 ns in drift time.

Azimuthal cathode pad or strip readout, included on the outer surfaces of the superlayers, is needed for bunch assignment since the propagation time along the wires is 16 ns for the longer outer layers. Azimuthal cathode pads or strips will also be useful in reducing stereo ambiguities. There are 15 superlayers in all for a total of 120 measurements. The total number of cells is 122,368. The total number of radiation lengths is 8% for a particle traversing the central tracking chambers at  $90^\circ$ . The Large Solenoid Detector central tracking system geometry is summarized

in Table I.<sup>10</sup> In order to provide momentum measurement for  $1.2 \lesssim |\eta| < 2.5$ , the Large Solenoid Detector included tracking in the intermediate region to take over where the central tracking ends. The intermediate tracking extends to  $\pm 4$  m along the beam line. Charged particles can be detected up to  $|\eta| \leq 3.0$ . The intermediate tracking consists of several superchambers, each with position measurements at several closely-spaced  $z$  values. Two options were considered: planes of parallel wires and radial chambers. Both options use cathode pads to read out the coordinate along the wires. The options for intermediate tracking have not yet been worked out in as much detail as the central tracking. Both require large numbers of readout channels.

The central and intermediate tracking systems for the Large Solenoid Detector are shown in Fig. 4. The entire Large Solenoid Detector is shown in Fig. 5. The momentum resolution for the Large Solenoid Detector as a function of polar angle and rapidity is shown in Fig. 6.

### 3. TRACKING SIMULATION

#### 3.1 Simulation of a Central Tracking System for the SSC

The SSC central tracking system design used for this simulation was based on that in the Large Solenoid Detector<sup>7</sup>), described in Section 2.3, although it is quite general and can be used for any system of cylindrically-oriented sensing elements. The central tracking system extended radially from 50 cm to 160 cm and covered  $|\eta| < 1.2-1.5$ . The cylindrical layers of wires parallel to the beam direction were grouped into superlayers with eight layers each. Within each superlayer the layers were staggered by half the cell width, as shown in Fig. 3. All parameters of the detector, such as number of superlayers, number of layers in each superlayer, minimum and maximum radius for each superlayer, length

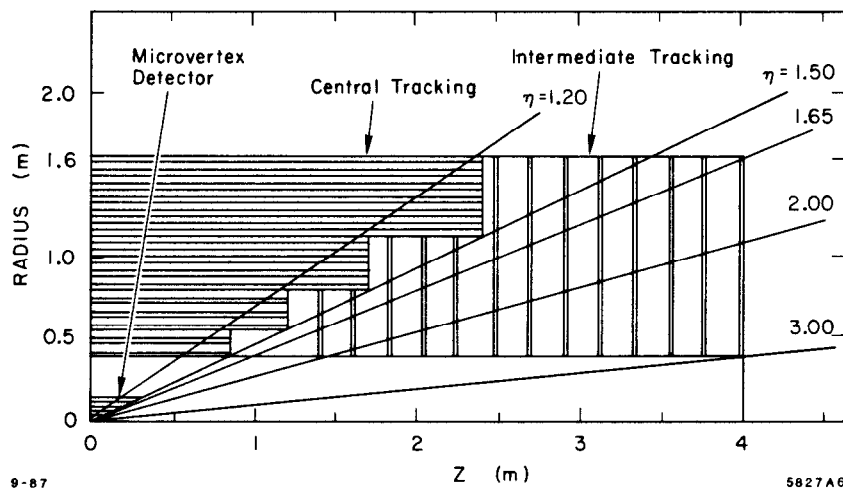


Fig. 4. Schematic view of central and intermediate tracking systems in the Large Solenoid Detector (from Ref. 7).

of each superlayer, and azimuthal spacing between sense wires can be specified independently. The parameters of the central tracking system used in this simulation are as shown in Table I, except that we included only the outer 13 superlayers. The design is based on a pattern recognition strategy of finding track segments in superlayers and then linking the segments to form tracks. Track segments in outer superlayers could be used in the trigger. We used a solenoidal magnetic field of 2 Tesla. The spatial resolution was taken to be  $150 \mu\text{m}$ . So far, we have simulated only axial wires, that is, wires parallel to the cylinder axis.

Table I. Summary of Large Solenoid Detector Central Tracking System (from Ref. 7)

Super-layer Number	Inner Radius (cm)	Module Thickness (cm)	Half Length (cm)	Straw Diameter (mm)	Rapidity Range	Cell Occupancy (%)
1	40	2.7	85.2	3.92	1.50	12.1
2	48	2.7	85.2	3.92	1.34	9.1
3	56	2.7	119.0	3.92	1.50	8.8
4	64	2.7	119.0	3.92	1.38	7.0
5	72	4.1	119.0	5.89	1.28	13.0
6	80	4.2	170.0	6.04	1.50	14.5
7	88	4.2	170.0	6.17	1.41	12.9
8	96	4.3	170.0	6.28	1.34	11.6
9	104	4.4	170.0	6.38	1.27	10.5
10	112	4.5	238.5	6.47	1.50	11.9
11	120	4.5	238.5	6.55	1.44	10.9
12	128	4.6	238.5	6.61	1.38	10.0
13	136	4.6	238.5	6.68	1.33	9.3
14	144	4.6	238.5	6.73	1.28	8.5
15	152	4.7	238.5	6.78	1.23	7.9

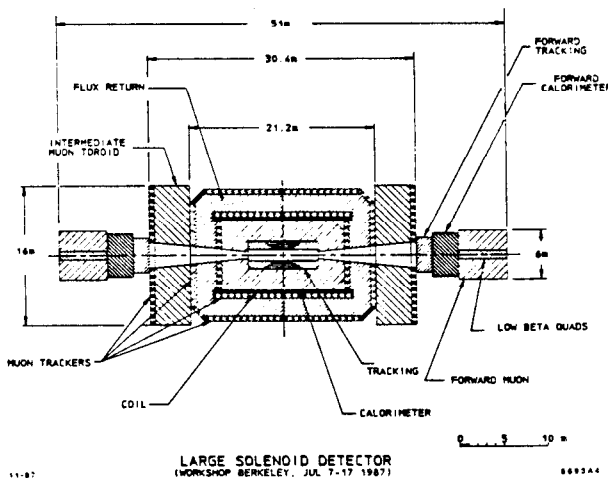


Fig. 5. Schematic view of the Large Solenoid Detector from the 1987 Berkeley Workshop.<sup>7)</sup>

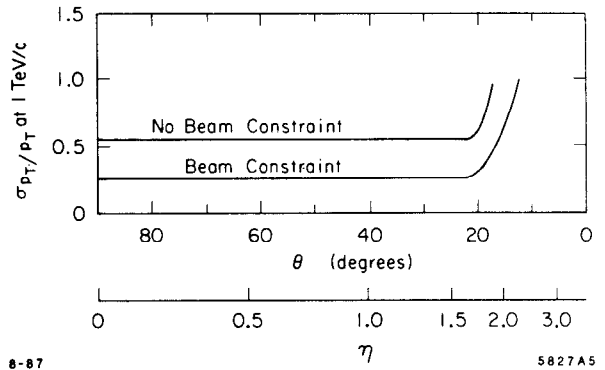


Fig. 6. Momentum resolution as a function of polar angle and rapidity in the Large Solenoid Detector for the 13 superlayers at radii  $> 50 \text{ cm}$  in the central tracking system and including intermediate tracking (from Ref. 7).

We used ISAJET<sup>11)</sup> to generate events from interesting physics processes, such as high- $p_T$  two jet events or Higgs boson production, and from inelastic scattering background, for which we used minimum bias events. We used the GEANT3<sup>12)</sup> general-purpose detector simulation package to simulate the interactions of the particles with the detector. One of the reasons for using GEANT3 was the hope that this tracking simulation software could be used with other GEANT-based subroutines to simulate SSC detectors. In fact, we have already realized some of the advantages of using a general-purpose detector simulation package in that we were able to use the GEANT3 environment, especially the graphics interface, set up by the SLD Collaboration on the SLAC IBM 3081 for their detector simulation.

Using GEANT, the particles interact in the 8% of a radiation length of material due to straw tube walls, wires, and gas<sup>7)</sup> (the material was assumed to be distributed uniformly throughout the tracking volume), including photon conversion and multiple Coulomb scattering. Charged particles are bent in the 2 T magnetic field. Every time a charged particle crossed a layer boundary, a hit was produced representing the distance of closest approach to the nearest sense wire. Only the radial volumes were specified in GEANT, not the azimuthally-spaced straw tubes, in order to save computer time. The drift distances were smeared according to a Gaussian distribution with width equal to the spatial resolution. The drift distances were then converted to drift times using a drift velocity of  $50 \mu\text{m}/\text{ns}$ . Digitizations were then produced representing a drift time and wire number for each track in each layer. If a track did not reach a layer because of bending in the magnetic field or leaving the tracking volume, no hit or digitization was produced. We included the background from inelastic scatterings in the same and out-of-time bunch crossings by superimposing the digitizations from mini-

mum bias events. We included the number of bunch crossings indicated by the resolving time of the straw tube cell. At each bunch crossing the number of events to be included was determined from a Poisson distribution with a mean of 1.6 interactions per bunch crossing. Drift times from background events were then increased or decreased by the time difference between the bunch crossing of the background event and the bunch crossing of the event of interest. The double-hit resolution was equal to the cell width, that is, only one hit was allowed per wire. We discarded all but the earliest hit with positive time. In addition, we removed digitizations in the tails of those from previous bunch crossings, that is, we assumed that a wire was dead for a time equivalent to the cell width. The simulation program is described in more detail in Ref. 13.

### 3.2 Results of the Simulation

We used the simulation described above to study tracking in SSC events. The first type of events we examined were high- $p_T$  ( $p_T > 1 \text{ TeV}/c$ ) two-jet events. Figure 7(a) shows such an event in the detector described in Section 2.3 with a 2 Tesla magnetic field. Figure 7(b) shows an enlargement of the same event in the outer two superlayers in the area of the dense jet. Figure 7(c) shows the earliest hits in the cells for the tracks shown in Fig. 7(b). When two tracks are close together, they produce hits only in every other layer because the cells in every other layer are staggered azimuthally so that one track passes closest to the sense wires in every other layer and the other track is closest in the alternate layers. Figures 7 and 8 do not show hits from background events or converted photons.

Some detector studies in the past have focused on non-magnetic detectors.<sup>14)</sup> Figure 8(a) shows the same event as in Fig. 7(a) with no magnetic field. Figure 8(b) shows the tracks and earliest hits in the cells in an enlarged region in the area of the dense jet in the outer two superlayers, as in Figs. 7(b) and (c).

Although we have not quantified these observations with high-statistics studies, we note:

1. Although these events have very dense jets which seem at first to be impossible to resolve, when viewed on the scale of the wire spacings most of the hits appear to lie on identifiable tracks with a 2 Tesla magnetic field, particularly in the outer superlayers.
2. Eight layers in a superlayer is probably close to the optimum number because two tracks which are as close as the wire spacings produce hits only on every other layer because of the staggering. Some of these hits may be lost due to nearby curling tracks or background hits. Three tracks within the wire spacing distance would not be resolvable.

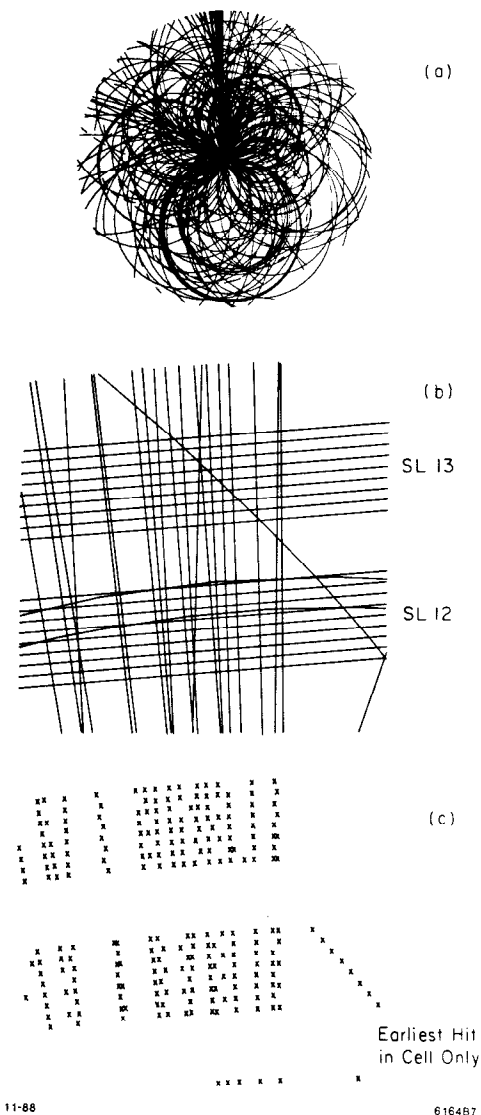


Fig. 7. (a) Two-jet event from ISAJET with  $p_T > 1 \text{ TeV}/c$  in a 2 Tesla magnetic field in a detector of the geometry of the Large Solenoid Detector. There are 223 particles with  $p_T > 200 \text{ MeV}/c$  and  $|\eta| < 1.5$ . Converted photons and background from minimum bias events are not shown. (b) Enlargement of the event in the outer two superlayers in the area of the dense jet at the top of the detector. (c) Earliest hit in each cell for the tracks shown in (b).

3. Although a 2 Tesla magnetic field produces curling tracks which obscure the high- $p_T$  tracks to some extent, particularly in the inner superlayers, the effect in the outer superlayers is to spread out the tracks and, of course, remove the low- $p_T$  tracks from consideration.

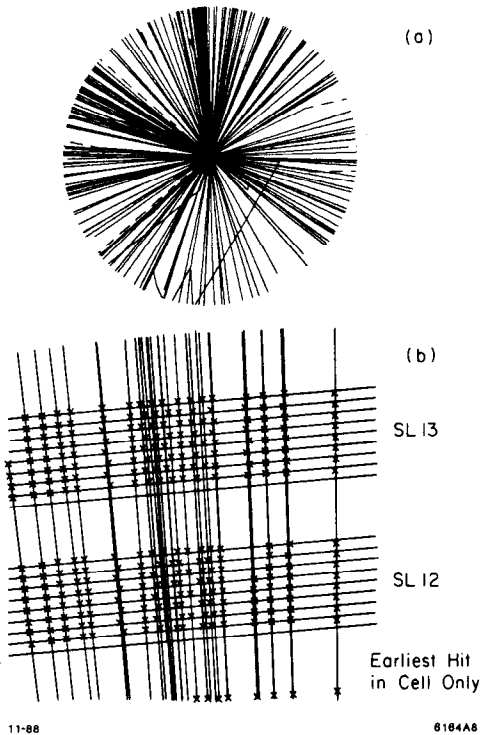


Fig. 8. (a) Same event as in Fig. 7(a) with no magnetic field. (b) Tracks and earliest hits in the cells in an enlarged region in the outer two superlayers in the area of the dense jet. Converted photons and background from minimum bias events are not shown.

We next turned our attention to events from Higgs boson production,  $pp \rightarrow HX$ , with the Higgs decaying to  $Z^0 Z^0$  and both  $Z^0$ 's decaying to  $e^+e^-$  or  $\mu^+\mu^-$ . We used a Higgs mass of  $400 \text{ GeV}/c^2$ . Such events allowed us to focus on the measurement of the high- $p_T$  particles from the Higgs decay. Any large solid angle SSC detector must be able to measure such events. Also, these events are not as trivial to deal with as might have been naïvely guessed. There are many tracks from the underlying event and from the particles recoiling against the Higgs boson, even before adding the hits from background interactions. For these events we used the full simulation as described in the previous Section. We generated  $\sim 200$  events. An example of a Higgs event in the simulated central tracking system is shown in Fig. 9. The leptons from the Higgs decay are indicated by the heavier lines.

The  $p_T$  distribution for all tracks in the Higgs events is shown in Fig. 10(a). Figure 10(b) shows the  $p_T$  distribution for leptons only. Nearly all of the tracks with  $p_T > 50 \text{ GeV}/c$  are the leptons from the Higgs decay. The fully-simulated events, including adding digitizations from minimum bias background events and removing digitizations within the double-hit resolution, had 12,000–25,000 digitizations, as shown in Fig. 11(a). The fraction of dig-

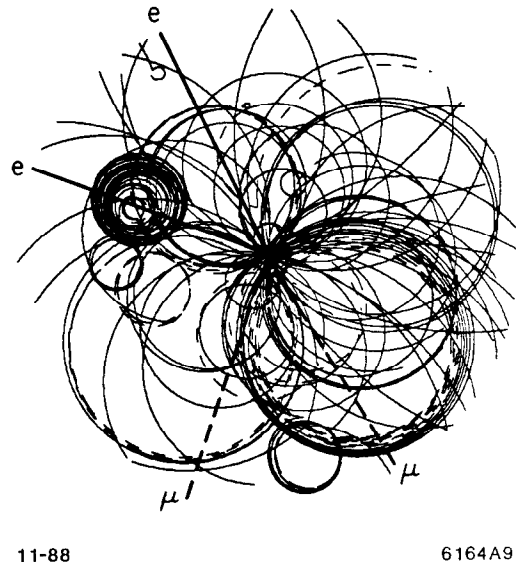


Fig. 9. Example of a Higgs event in the simulated central tracking system. The leptons from the Higgs decay are indicated by the heavier lines. Converted photons and other interactions with the material are included.

itizations from the minimum bias background events is shown in Fig. 11(b). On the average 57% of the digitizations were due to background events. The fraction of digitizations lost for all tracks in the Higgs events as a function of superlayer is shown in Fig. 12(a). On the average  $\sim 12\%$  of the digitizations were lost because of the double-hit resolution, and the loss was about the same in all superlayers. The fraction of digitizations lost for the leptons from the Higgs decay is shown in Fig. 12(b). An average of 7.3% of the digitizations were lost for the leptons from the Higgs decay with the worst losses being in the superlayers at 70–90 cm radius, presumably because of curling tracks.

### 3.3 Pattern Recognition

We began working on pattern recognition algorithms in order to examine our original design goals of finding track segments in superlayers and removing hits from out-of-time bunch crossings. We also wanted to make the algorithm simple with the hope of using it in the trigger. The algorithm for finding track segments was the following:

1. In each superlayer we identified "roads" containing hits. There are two parameters which can be varied: the width of the road and the number of hits required on the road. We used a width of 5 wires (22 mrad in the outer superlayer) and required 3 or more hits out of 8 possible. For isolated tracks one could require more hits; however, if two tracks are close together, as in Fig. 7, they will produce hits only on alternate

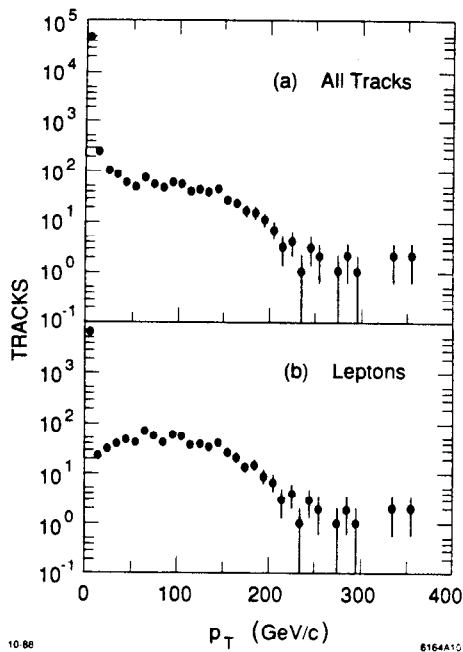


Fig. 10. (a)  $p_T$  distribution for all tracks in the Higgs events. (b)  $p_T$  distribution for the leptons in the Higgs events.

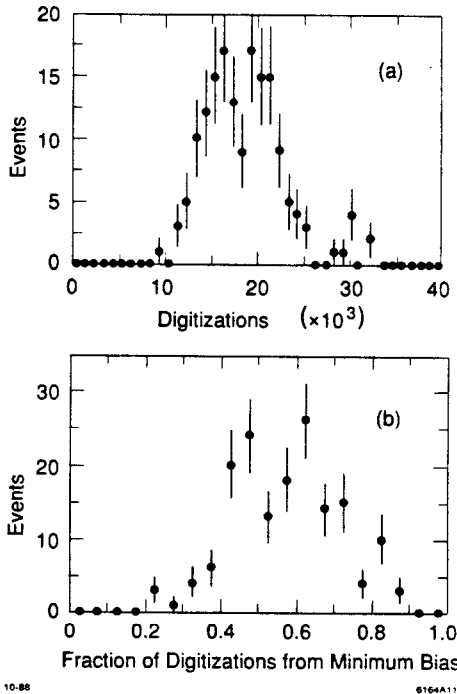


Fig. 11. (a) Total number of digitizations in Higgs events, including digitizations from minimum bias background events. (b) Fraction of digitizations from the minimum bias background events. The mean is  $0.572 \pm 0.011$ .

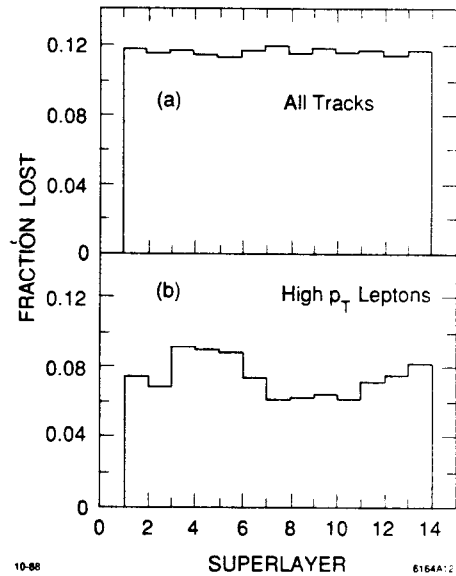


Fig. 12. (a) Fraction of digitizations lost for all tracks in the Higgs events as a function of superlayer. The mean is  $(11.58 \pm 0.65)\%$ . (b) Fraction of digitizations lost for the leptons from the Higgs decay as a function of superlayer. The mean is  $(7.93 \pm 0.61)\%$ .

layers and if one is lost due to the double-hit resolution there will be only 3 hits. The road requirement discriminates against low- $p_T$  tracks.

2. We required that at least one of the hits be in a layer with the opposite wire stagger from the others so that the left-right ambiguities could be resolved and hits from out-of-time bunch crossings rejected.
3. We required that the hits be consistent with a straight line to within an error and in the process resolved the left-right ambiguities. Of course, the tracks approximate straight lines only locally within the superlayer, and the spatial resolution must also be taken into account.

Figure 13(a) shows all of the digitizations<sup>15)</sup> for the event shown in Fig. 9, including those from minimum bias background events. Figure 13(b) shows only those digitizations which are included in segments. Keeping only those digitizations which form segments cleans up the events considerably. Figure 13(c) shows the tracks from the original event in the outer five superlayers in the region around the muon at the lower right. Figure 13(d) shows all of the digitizations in the event in the enlarged region (the digitizations are displayed at the locations of the hit wires). Finally, Fig. 13(e) shows only those digitizations which form track segments; here, the left-right ambiguities have been resolved, the drift times have been converted to distances, and the digitizations are displayed at the positions of closest approach of the tracks to the wires. One can

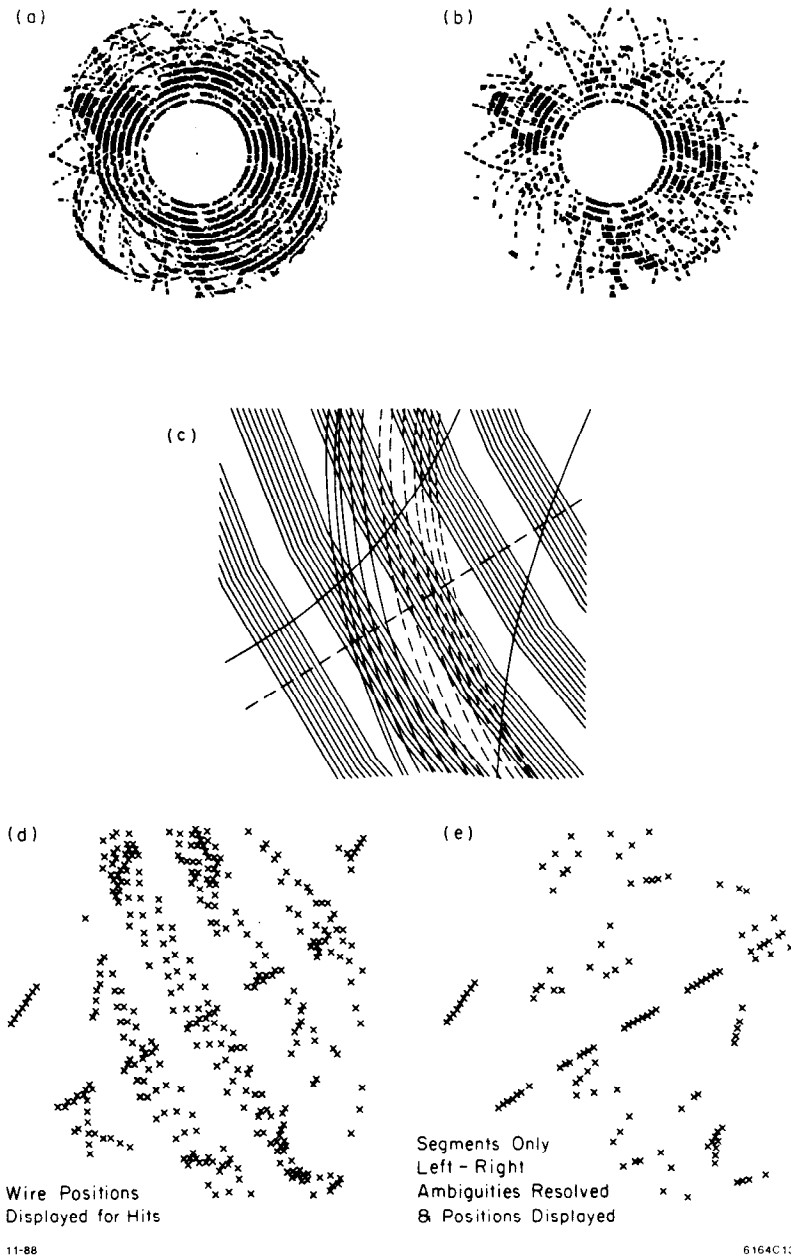


Fig. 13. (a) All of the digitizations for the Higgs event shown in Fig. 9, including those from minimum bias background events. (b) Digitizations for this event which are included in track segments, as defined in the text. (c) Tracks from the original event in an enlarged region in the outer five superlayers in the region around the muon at the lower right. (d) All of the digitizations in the event in the enlarged region of (c) (the digitizations are displayed at the locations of the hit wires). (e) Only those digitizations which form track segments in the enlarged region. Here, the left-right ambiguities have been resolved, the drift times have been converted to distances, and the digitizations are displayed at the positions of closest approach of the tracks to the wires.

Depending on the effects on the physics analyses, we might envision making this requirement at the processor level, reading out only the hits that form track segments.

clearly identify the muon track, and most of the extra hits have been removed.

Next, we applied our segment-finding algorithm to the  $e$  and  $\mu$  tracks from Higgs boson decays. We defined two classes of segments: a "good" segment was one with at least five hits from a lepton track and no other hits, and an "OK" segment was one with at least five hits from the lepton track and one hit from another track. The effects of hits from other tracks remain to be studied; however, since all of the hits were consistent with a straight line we would expect the segment with one hit from another track to give nearly the same fitted straight line segment as it would without the hit. Besides, in reality, we will not know which hits are from which tracks. We will compare measured momenta with produced momenta in future studies. With these definitions, we counted the number of segments found for each lepton track. As an example, Table II gives the number of segments found for each of the four lepton tracks in the event shown in Figs. 9 and 13. The maximum number of segments is 13, the number of superlayers. As we shall see, this event is rather typical.

Table II. Segments Found for Four Lepton Tracks in Sample Event

$e$ or $\mu$ Track	Good Segments	Total (Good or OK) Segments
1	4	9
2	8	11
3	5	8
4	9	11

The distribution of the number of good segments for the  $e$ 's and  $\mu$ 's in the Higgs events is shown in Fig. 14(a). The corresponding distribution of total (good or OK) segments is shown in Fig. 14(b). We see that the lepton tracks from Higgs decay have an average of about 8 good segments and 10 total segments out of 13 possible. Figure 15(a) shows the fraction of segments which are good as a function of superlayer number, whereas Fig. 15(b) shows the same distribution for the fraction of segments which are either good or OK. Typically 30–50% of segments were good in the inner superlayers, increasing to almost 80% for the outer superlayers. When OK segments are counted as well, 50–60% of segments are accepted for inner superlayers and over 80% for outer superlayers. Segments were most likely to be lost in the superlayers at 70–90 cm, as noted in the previous Section for hits lost.

### 3.4 Future Work

We are planning to continue our tracking simulation studies using the software we have developed. Future work will include:

1. Continued studies of pattern recognition and track finding along the lines described in previous Sections, including linking the segments to form tracks.

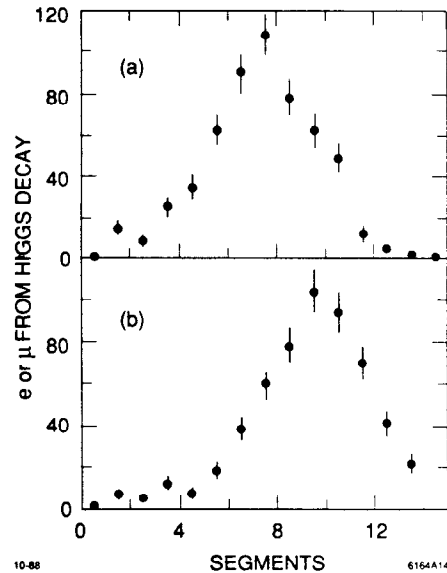


Fig. 14. (a) Distribution of the number of good segments out of 13 possible for the  $e$ 's and  $\mu$ 's from the Higgs decays. (b) Distribution of the number of total segments (good or OK) for the leptons from the Higgs decay.

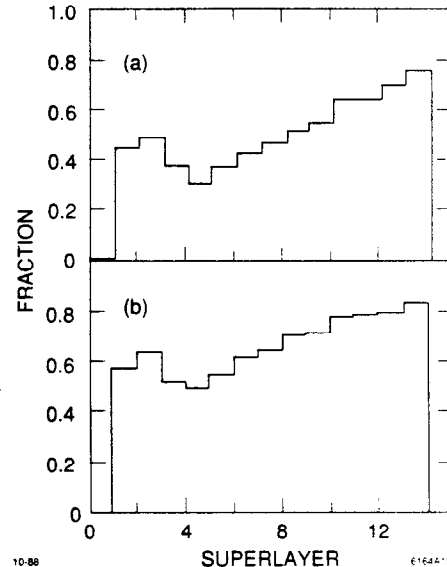


Fig. 15. (a) Fraction of segments which are good as a function of superlayer number for the lepton tracks from the Higgs decay. (b) Fraction of segments which are either good or OK as a function of superlayer.

2. Simulation of small-angle stereo wires and cathode strips for reconstruction of the direction along the wires. Stereo segments can then be found in the same manner as axial segments, and the stereo segments can be linked to axial segments to form tracks. At this point we will be able to study how much ad-

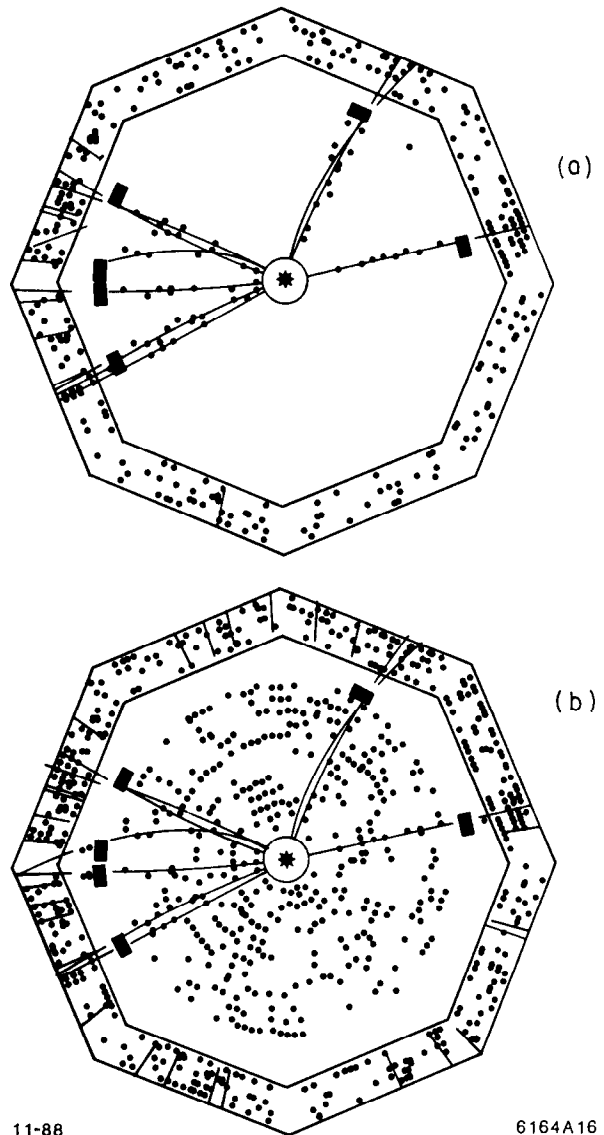
ditional information from cathode strips is needed in order to link the stereo hits.

3. A more realistic simulation of electron drift in small-cell or straw tube drift chambers is needed, including the effects of  $\mathbf{E} \times \mathbf{B}$ . For the study described here we have used only the geometric distance of closest approach.
4. Conceptual design and simulation of intermediate tracking,<sup>7)</sup> ( $1.2 < |\eta| < 2.5$ ) as described briefly in Section 2.3.
5. Tracking studies for different physics processes, such as new heavy fermions, supersymmetric particles, and high- $p_T$  two-jet events.
6. Vary tracking system parameters such as cell radius to determine the effects on pattern recognition and tracking efficiency.
7. Begin to develop a realistic design for a tracking system for a complete SSC detector, including other detector components.

#### 4. CONCLUSIONS

We have shown that an SSC tracking system design based on a pattern recognition strategy of finding track segments in superlayers appears to provide a powerful means of finding tracks in complex SSC events, even in an environment of multiple events from several bunch crossings. So far, detailed simulations have verified the concepts developed over several years for SSC tracking detectors. Although a great deal of work remains to be done, we are hopeful that an SSC tracking system based on conventional wire chambers will enable us to explore the new physics which awaits us in the SSC regime.

As an example of an existing tracking detector based on track segment finding, we show in Fig. 16(a) a Monte Carlo simulation of a multihadronic  $Z^0$  decay in the Mark II central drift chamber.<sup>16)</sup> Figure 16(b) shows a real SLC background event superimposed on the  $Z^0$  event. The background event has an occupancy of  $\sim 50\%$ . Also shown in Figs. 16(a) and (b) are the tracks found by the standard Mark II pattern recognition and track fitting programs. Even in the presence of the very high background occupancy, the original tracks can be found with reasonably high precision. The Mark II detector would not take data under these circumstances because other parts of the detector, in particular, the calorimeters and time-of-flight scintillation counters, cannot operate with such high backgrounds. The SLC backgrounds originate from a much different source than SSC backgrounds, namely tails of the beam scraping various apertures. The Mark II central drift chamber, which is a wide cell jet chamber, would not be able to operate in the SSC environment. Nevertheless, this example shows the power of track segment finding in a high background situation. Another point which can be



11-88

6164A16

Fig. 16. (a) Monte Carlo simulation of a multihadronic  $Z^0$  decay in the Mark II central drift chamber. (b) Real background event from the SLC superimposed on the  $Z^0$  event. The background event has  $\sim 50\%$  occupancy. Also shown in (a) and (b) are the tracks found by the standard Mark II pattern recognition and track fitting programs.

made is that very high energy  $e^+e^-$  linear colliders which can probe physics in the same energy region as the SSC will be even more susceptible to backgrounds of the SLC type. Although the interactions themselves may be much cleaner than at the SSC, the backgrounds have the potential of being much worse. In either the SSC environment or at high-energy  $e^+e^-$  linear colliders a tracking system based on track segment finding has the best capability of surviving and yielding tracks in high background situations.

## ACKNOWLEDGMENTS

We would like to thank members of the SLD Collaboration at SLAC, especially Dave Aston, for their help in getting GEANT running on the SLAC IBM computer and for providing the interface to GEANT graphics. We wish to thank Gil Gilchriese for organizing such a stimulating and informative conference. We gratefully acknowledge the support of the Department of Energy Program for Generic Detector Research and Development for the SSC.

## REFERENCES

- 1) D. G. Cassel, G. G. Hanson *et al.*, "Report of the Central Tracking Group," in *Proceedings of the 1986 Summer Study on the Physics of the Superconducting Supercollider*, edited by R. Donaldson and J. Marx, Snowmass, CO, 1986, p. 377.
- 2) *Radiation Levels in the SSC Interaction Regions*, Task Force Report, edited by D. E. Groom, SSC-SR-1033, SSC Central Design Group, June, 1988.
- 3) *Report of the Task Force on Detector R&D for the Superconducting Super Collider*, SSC-SR-1021, SSC Central Design Group, June, 1986, pp. 44-60; M. G. D. Gilchriese, in *Proceedings of the 1984 Summer Study on the Design and Utilization of the Superconducting Super Collider*, edited by R. Donaldson and J. G. Morfin, Snowmass, CO, 1984, p. 607; G. Hanson and D. Meyer, *ibid.*, p. 585.
- 4) J. Va'vra, in *Proceedings of the Workshop on Radiation Damage to Wire Chambers*, edited by J. Kadyk, Lawrence Berkeley Laboratory, Berkeley, CA, 1986, p. 263.
- 5) A. H. Walenta, Nucl. Instr. and Meth. **217**, 65 (1983).
- 6) R. Thun, "Prospects for Wire Chambers at High Luminosity," in these Proceedings.
- 7) G. G. Hanson, S. Mori, L. G. Pondrom, H. H. Williams *et al.*, "Report of the Large Solenoid Detector Group," in *Proceedings of the Workshop on Experiments, Detectors, and Experimental Areas for the Supercollider*, edited by R. Donaldson and M. G. D. Gilchriese, Berkeley, CA, 1987, p. 340.
- 8) R. L. Gluckstern, Nucl. Instr. and Meth. **24**, 381 (1963).
- 9) R. DeSalvo, "A Proposal for an SSC Central Tracking Detector," CLNS 87/52.
- 10) The cell occupancies have been increased from those in Ref. 7 to reflect the increase of the number of charged particles per unit rapidity from 6 to 7.5.
- 11) F. E. Paige and S. D. Protopopescu, "ISAJET 5.30: A Monte Carlo Event Generator for  $pp$  and  $p\bar{p}$  Interactions," in *Proceedings of the 1986 Summer Study on the Physics of the Superconducting Supercollider*, edited by R. Donaldson and J. Marx, Snowmass, CO, 1986, p. 320. (The current version of ISAJET is 6.12.)
- 12) R. Brun, F. Bruyant and A. C. McPherson, *GEANT3 User's Guide*, CERN DD/EE/84-1.
- 13) A. P. T. Palounek, "Simulating a Central Drift Chamber for a Large Solenoid Detector at the SSC," SLAC-PUB-4787.
- 14) T. Åkesson *et al.*, "Report of the Non-magnetic Detector Group," in *Proceedings of the Workshop on Experiments, Detectors, and Experimental Areas for the Supercollider*, edited by R. Donaldson and M. G. D. Gilchriese, Berkeley, CA, 1987, p. 472.
- 15) The GEANT3 graphics does not display digitizations, only hits. To display digitizations, they must be converted to spatial coordinates and stored in the hit bank.
- 16) G. Hanson, "The New Drift Chamber for the Mark II Detector at the SLAC Linear Collider," in *Proceedings of the Fourth International Wire Chamber Conference, Vienna, Austria, 1986*, Nucl. Instr. and Meth. **A252**, 343 (1986).